Crystallographic Studies on Endothelial Nitric Oxide Synthase Complexed with Nitric Oxide and Mechanism-Based Inhibitors†

Huiying Li,‡,§ C. S. Raman,‡,§,|| Pavel Martásek,⊥ Bettie Sue S. Masters,⊥ and Thomas L. Poulos*,‡

Departments of Molecular Biology & Biochemistry and Physiology & Biophysics and Program in Macromolecular Structure, University of California, Irvine, California 92697-3900, and Department of Biochemistry, University of Texas Health Science Center, San Antonio, Texas 78229-3900

Received November 20, 2000; Revised Manuscript Received January 19, 2001

ABSTRACT: The crystal structure of the endothelial nitric oxide synthase (NOS) heme domain complexed with NO reveals close hydrogen bonding interactions between NO and the terminal guanidino nitrogen of the substrate, L-arginine. Dioxygen is expected to bind in a similar mode which will facilitate proton abstraction from L-Arg to dioxygen, a required step for O−O bond cleavage. Structures of mechanism-based NOS inhibitors, N^5-(1-iminoethyl)-L-ornithine and *N*-(3-(aminomethyl)benzyl)acetamidine, provide clues on how this class of compounds operate as suicide substrate inhibitors leading to heme oxidation.

NO is an important mediator of a wide range of physiological and pathophysiological processes in humans and other mammals (*1*−*3*). The formation of NO is catalyzed by nitric oxide synthases (NOS)[1] in the following reaction:

$$\text{L-Arg} + 2O_2 + 1.5\text{NADPH} + 2H^+ \rightarrow \text{L-citrulline} + \bullet\text{NO} + 2H_2O + 1.5\text{NADP}^+$$

The three genetically encoded mammalian NOS isoforms, neuronal NOS (nNOS), inducible NOS (iNOS), and endothelial NOS (eNOS) share a similar modular architecture (*4*, *5*). The C-terminal domain is homologous to NADPH-cytochrome P450 reductase and contains bound FMN and FAD and a binding motif for NADPH (*6*). The N-terminal domain contains binding sites for the essential cofactor, tetrahydrobiopterin, the heme prosthetic group, and the substrate, L-Arg. These two major functional domains of NOS are linked by a calmodulin-binding motif. All three isoforms share as high as 50% sequence identity. The N-terminal segment, particularly of the constitutive isoforms, exhibits the largest variation in sequence. While the N-terminal segments are not essential for catalytic activity, they are involved in cellular targeting and protein−protein interactions. Very recently, the crystal structure of the N-terminal PDZ domain of nNOS in complex with syntrophin was determined (*7*).

All three NOS isoforms catalyze NO production via an identical two-step mechanism. The substrate, L-Arg, is first converted to N^G-hydroxy-L-Arg (NHA) at the heme active site. In the second step, NHA is further oxidized at the heme site to NO and citrulline (*2*). Reducing equivalents required for catalysis are transferred from NADPH through FAD to FMN and finally to the heme. Both constitutively expressed isoforms, eNOS and nNOS, are regulated by the binding of calmodulin to the linker connecting the heme and flavin domains, resulting in the stimulation of electron transfer to the heme. Inducible NOS (iNOS), however, contains permanently bound calmodulin (*8*) and also exhibits the highest turnover among the three isoforms (*9*).

All three NOS isoforms are functional only as a tight homodimer through interactions between the heme domains. The dimeric structure of the heme domain and its requirement for formation of the pterin binding site has been revealed by the crystal structures of the heme domain for iNOS (*10*−*12*), eNOS (*11*, *13*), and nNOS (unpublished). In addition, a Zn-tetrathiolate center at the dimer interface aids in dimer stabilization and formation of the pterin binding site (*13*). H_4B, the fully reduced form of biopterin, is essential for enzymatic activity (*14*) and, in the absence of H_4B, NOS generates excess amounts of superoxide (*15*−*17*). The final products of turnover by H_4B-free iNOS were found to be NO^-, rather than NO, and cyanoornithine as a side product, in addition to citrulline (*18*). One possible role for H_4B is to serve as a one-electron donor to the heme iron, which is required for cleavage of the O−O bond (*13*, *19*). Recent freeze-quench EPR studies show that the pterin in the iNOS heme domain does indeed form a radical and that radical formation correlates with the formation of the first product, N^G-hydroxy-L-Arg (*20*).

Similar to cytochrome P450 chemistry, dioxygen binding to the reduced heme iron and subsequent O−O bond

† This work was supported by NIH grants GM 57353 (TLP) and GM52419 (BSSM) and Robert A. Welch Grant No. AQ-1192 (BSSM). During this work C. S. Raman was a fellow of the American Heart Association (Western States Affiliate). We gratefully acknowledge the assistance provided by the staff at SSRL BL7-1 during data collection.

* To whom correspondence should be addressed. E-mail: poulos@uci.edu. Phone: (949) 824-7020. Fax: (949) 824-3280.

‡ University of California.

§ These authors contributed equally to this work.

|| Present address: Structural Biology Center, Department of Biochemistry and Molecular Biology, University of Texas Medical School, 6431 Fannin, Houston, TX 77030.

⊥ University of Texas Health Science Center.

[1] Abbreviations: NO, nitric oxide; NOS, nitric oxide synthase; NIO, N^5-(1-iminoethyl)-L-ornithine; 1400W, trivial name for *N*-(3-(aminomethyl)benzyl)acetamidine; L-Arg, L-arginine; L-Cit, L-citrulline; NHA, N^G-hydroxy-L-arginine; NMMA, N^G-monomethyl-L-arginine.

10.1021/bi002658v CCC: $20.00
Published on Web 04/12/2001

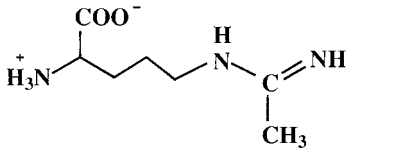

L-NIO

N^5-(1-iminoethyl)-L-ornithine

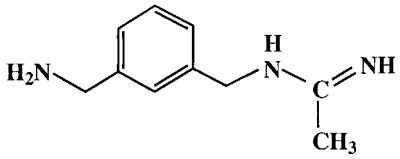

1400W

N-(3-(aminomethyl)benzyl)acetamidine

FIGURE 1: Structures of L-NIO and 1400W used in this study.

cleavage are thought to be key steps in determining whether the catalytic reaction proceeds normally to NO production or is "uncoupled" to produce superoxide or peroxide. This kind of uncoupling is often found to correlate with the inactivation of NOS by so-called mechanism-based inhibitors (*21*−*23*). Another type of inhibition unique to NOS is binding of the self-generated NO to the heme iron before it can be removed by incoming dioxygen (*24*). To understand the stereochemical details of diatomic ligand binding to NOS and suicide substrate inhibition, we have determined the eNOS heme domain crystal structure complexed with NO and two mechanism-based inhibitors, N^5-(1-iminoethyl)-L-ornithine (L-NIO) and *N*-(3-(aminomethyl)benzyl)acetamidine (1400W).

MATERIALS AND METHODS

Materials. Both NIO and 1400W (structures shown in Figure 1) were purchased from Alexis. The heme domain of bovine eNOS was generated by trypsinolysis of the recombinant holoenzyme expressed in *Escherichia coli* and purified as described (*25*). The pterin-free sample was prepared by omitting H_4B in all the buffers used during purification.

Crystal Growth. Crystals of eNOS heme domain were grown using the sitting drop method according to Raman et al. (*13*). The NIO complexed crystals were grown in the presence of 1 mM NIO in the crystallization cocktail, whereas the 1400W complex was prepared by soaking the eNOS-substrate complex crystals with 7 mM 1400W, solubilized in the cryoprotectant solution for 4 h prior to data collection.

Generation of NO Complexes. Crystals of the eNOS-substrate complex (H_4B-free or -bound) were passed stepwise through the artificial mother liquor containing increasing concentrations of cryoprotectant (*13*). The cryoprotectant-solution and the cryo-soaked crystals were subjected to anaerobic treatment by cycling between extensive degassing and purging with pure N_2 gas for 30−60 min. Fresh dithionite and sodium nitrite solutions were made with the degassed cryoprotectant-solution in sealed serum vials. NO-complexed crystals were prepared by soaking with 10 mM dithionite and 5 mM sodium nitrite for 50 min inside a glovebox before being flash frozen for data collections.

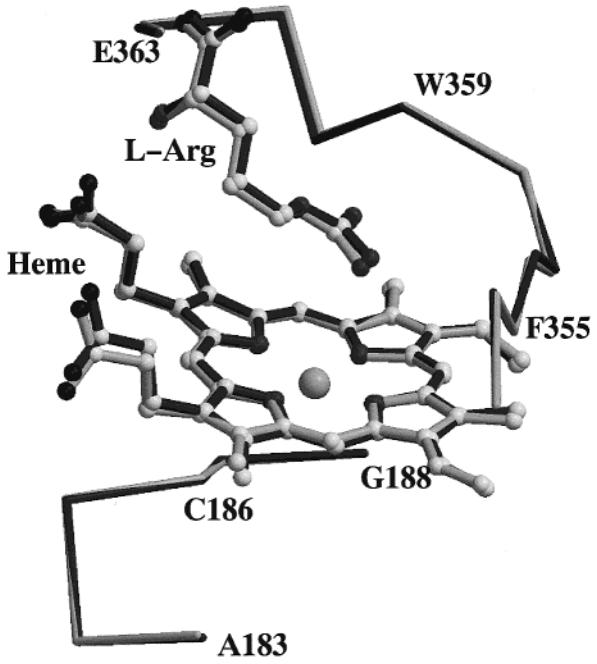

FIGURE 2: Superimposition of eNOS−substrate complex structures in the resting, oxidized (Fe^{3+}) state (PDB code 4NSE, dark color) and in the reduced (Fe^{2+}) state (PDB code 1FOL, light gray). The substrate moves in closer to the heme plane in the ferrous oxidation state, while the protein backbones, α-carbons of residues 183−188 and 353−363 shown, are essentially unchanged.

X-ray Diffraction Data Collection, Processing, and Model Refinement. All X-ray diffraction data reported here were collected at SSRL BL7-1 with a MarResearch Mar345 imaging plate at 100 K. Raw data were processed with the HKL suite (*26*). The eNOS heme domain model with all active site ligands removed was used for the initial electron density calculations with CNS (*27*). Subsequently, TOM/FRODO (*28*) was used for analyzing new structures and model building. Models were further refined and water molecules were picked up with the automatic routine in CNS and visually inspected. The proline-rich surface loop, residues 108−121, remained disordered in all structures and is tentatively modeled. The data collection and refinement statistics of all five structures are summarized in Table 1.

RESULTS

eNOS Heme Domain in the Ferrous State. To distinguish between alterations resulting from NO binding as opposed to reduction of the heme iron, the structure of the substrate-bound eNOS heme domain in the reduced state was determined. Heme reduction does not cause any conformational change in the protein portion of the structure, and the heme position relative to the surrounding protein backbone also remains approximately the same. However, the substrate does move closer to the heme by about 0.4−0.5 Å in both subunits of the dimer. The distance between the terminal guanidino nitrogen of L-Arg and the heme iron decreases from 4.36 Å in the oxidized state to 3.89 Å in the reduced state in subunit A and from 3.77 to 3.41 Å in subunit B (Figure 2). A certain degree of flexibility of the substrate in the active site has been observed before in other L-Arg-complexed eNOS heme domain structures (PDB code 4NSE). The substrate position relative to the heme plane varies slightly in the two subunits, where the distance of the L-Arg

Table 1: Data Collection and Refinement Statistics

data set	ferrous(−H_4B)	NO(−H_4B)	NO(+H_4B)	NIO	1400W
PDB code	1FOL	1FOO	1FOP	1ED6	1FOI
cell dimensions (Å)	$a = 58.23$	$a = 58.20$	$a = 58.55$	$a = 59.12$	$a = 58.46$
(SG: $P2_12_12_1$)	$b = 106.28$	$b = 106.56$	$b = 106.25$	$b = 106.16$	$b = 106.32$
	$c = 156.29$	$c = 156.67$	$c = 156.74$	$c = 156.70$	$c = 156.33$
data resolution (Å)	2.20	2.00	2.30	2.05	1.93
total observations	148 722	233 441	140 039	149 515	325 963
unique reflections	48 840	63 202	43 826	56 488	67 396
R_{sym}[a]	0.073	0.066	0.073	0.068	0.068
	(0.644)[b]	(0.571)	(0.725)	(0.769)	(0.626)
$\langle I/\sigma \rangle$	7.6	7.0	7.3	8.0	9.1
	(1.6)[b]	(1.7)	(1.2)	(1.4)	(2.1)
completeness	0.960	0.968	0.978	0.903	0.898
	(0.959)[b]	(0.962)	(0.985)	(0.882)	(0.864)
reflection used in refinement	39 326	60 791	34 789	56 388	63 078
R-factor[c]	0.222	0.223	0.220	0.241	0.223
R-free[d]	0.265	0.253	0.277	0.275	0.251
no. of protein atoms	6593	6593	6593	6593	6593
no. of heteroatoms	143	143	175	135	135
no. of waters	336	513	279	377	655
RMS deviation					
bond length (Å)	0.007	0.006	0.007	0.008	0.007
bond angle (deg)	1.4	1.3	1.4	1.4	1.3

[a] $R_{sym} = \sum|I - \langle I \rangle|/\sum I$, where I is the observed intensity and $\langle I \rangle$ the averaged intensity of multiple symmetry related observations of the reflection. [b] The values in parentheses were obtained in the outermost resolution shell. [c] *R*-factor $= \sum||F_o| - |F_c||/\sum|F_o|$, F_o and F_c are the observed and calculated structure factors, respectively. [d] *R*-free was calculated with 5% of reflections set aside randomly throughout the refinement. The same set of reflections were chosen for every data set.

Table 2: Stereochemistry of NOS Complexes at the Heme Active Site[a]

crystal	PDB code	bend angle (deg)[b]	Fe-X[c] (Å)	N−O[c] (Å)	O−NH1[d] (Å)	NH2−OE1[e] (Å)	NE-OE2[f] (Å)	NH1−Fe[g] (Å)
NO(−H4B)	1FOO	20	1.79	1.15	2.72	2.64	2.47	4.25
			1.80	1.13	2.73	2.71	2.56	4.30
NO(+H4B)	1FOP	20	1.79	1.15	2.72	3.09	2.77	4.28
			1.80	1.15	2.76	3.11	2.81	4.46
Fe3+(−H4B)	4NSE					3.02	2.80	4.36
						2.96	2.89	3.77
Fe2+(−H4B)	1FOL					2.94	2.53	3.89
						3.04	2.78	3.41

[a] The two numbers for each parameter refers to each subunit in the eNOS heme domain dimer. [b] Angle between the diatomic bond and the normal of the heme plane. [c] Bond between the heme iron and diatomic ligand, Fe-X, or that between two atoms of NO. [d] Hydrogen bonding distance from the oxygen of the diatomic ligand to the guanidino nitrogen, NH1, of L-Arg. [e] Hydrogen bonding distance from the guanidino nitrogen, NH2, of L-Arg to the carboxylate oxygen, OE1, of Glu363. [f] Hydrogen bonding distance from the guanidino bridging nitrogen, NE, of L-Arg to the carboxylate oxygen, OE2, of Glu363. [g] Distance from the guanidino nitrogen, NH1, of L-Arg to the heme iron.

terminal NH1 guanidino nitrogen to the heme iron is 4.36 Å in subunit A and 3.77 Å in subunit B (Table 2). However, in the structure of the reduced form, this 0.4−0.5 Å movement of substrate toward the heme iron is consistently observed in both subunits and is significant considering the rms deviations of the protein backbone atoms surrounding the heme are less than 0.2 Å when the structures in two different oxidation states are superimposed (Figure 2). The decrease of positive charge on the heme iron in being reduced from Fe^{3+} to Fe^{2+} possibly allows the positively charged L-Arg guanidinium to move closer to the iron for more favorable nonbonded contacts.

NO Complex. The NO complex of eNOS heme domain in the reduced state has been prepared with both tetrahydrobiopterin (H_4B)-free and -bound protein samples and L-Arg bound at the active site in both structures. Similar geometry of bound NO and interactions with L-Arg is found in both structures (Table 2) indicating that the pterin has little influence on NO binding geometry as long as L-Arg is bound at the active site. The binding of H_4B affects mainly the positions of both the Trp 449 indole ring and heme propionate groups, although the heme plane itself also has shifted slightly. Changes in protein backbone upon NO binding, however, are negligible.

NO binds end-on to the heme iron (Figure 3) with a 20° bend angle (Table 2) from the normal of the heme plane such that NO leans toward the *meso*-carbon between pyrrole rings C and D. As a result, the NO oxygen makes a van der Waals contact (3.7−3.8 Å) with Phe 355 and a hydrogen bond with the guanidino nitrogen (2.7−2.8 Å). To accommodate NO, the guanidino group of L-Arg moves closer to the Glu 363 side chain (Figure 4).

NIO Complex. Figure 5 shows the $2F_o - F_c$ electron density omit maps for the binding of both NIO and 1400W. As expected, NIO was found in the substrate binding site above the heme plane entertaining all the hydrogen bonding interactions observed between L-Arg and surrounding protein groups (Figure 6). The nitrogen atoms of the amidino group donates hydrogen bonds to the Glu 363 carboxylate side chain and the Trp 358 carbonyl oxygen exactly as in the L-Arg−enzyme complex. The conformation of the NIO molecule resembles that of L-Arg so closely that the Cδ atom

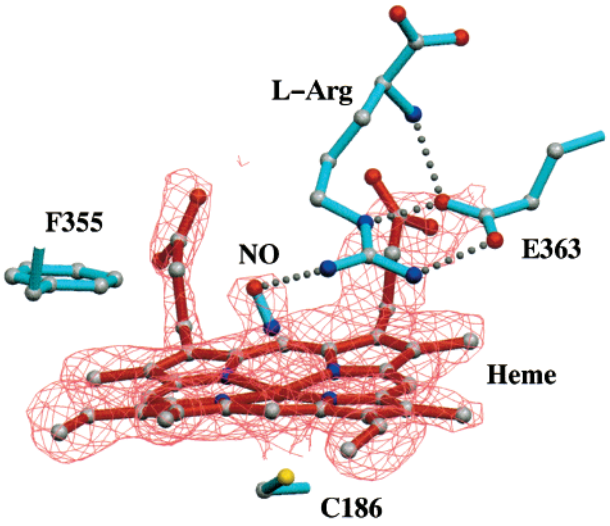

FIGURE 3: $2F_o - F_c$ omit map (contoured at 1σ) of the NO-substrate ternary complexes of eNOS heme domain. The hydrogen bonds are indicated by dotted lines. The atom color schemes are carbon, gray; oxygen, red; nitrogen, blue; sulfur, yellow.

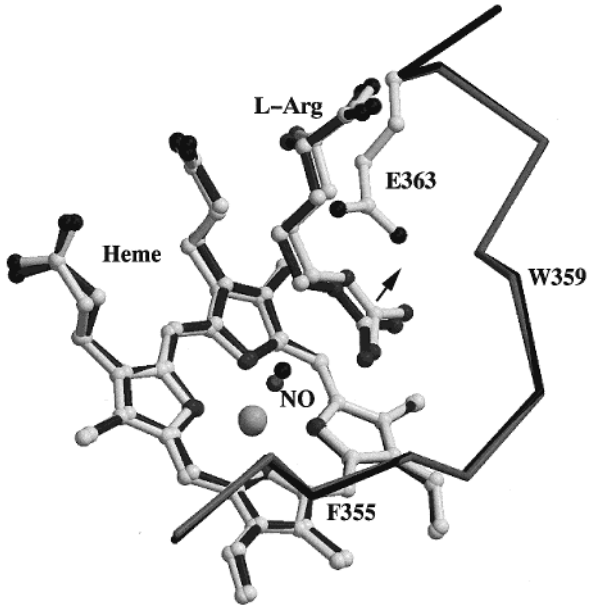

FIGURE 4: Superimposition of the NO-bound (PDB code 1FOO, light gray) versus NO-free (PDB code 4NSE, black) eNOS-substrate complex structures illustrating the shift (~0.4−0.5 Å) of substrate toward Glu363 side chain, shown by an arrow, upon NO binding. Changes in the protein backbones, shown as Cα trace for residues 353−364, are minimal.

is coplanar with the amidino group as it is in the guanidino group of L-Arg. The amidine methyl group is ~4.1 Å away from the heme iron. The closest contact of NIO to heme is between the NIO methyl carbon and the nitrogen of pyrrole ring B at 3.6−3.7 Å, while the distance to the α-*meso*-carbon of heme is less than 4.0 Å (Figure 6). It is interesting to note that a bridging water molecule normally found in the active site between the Pro 336 carbonyl oxygen and the guanidino nitrogen of substrate, is absent in the NIO complex structure. The lack of hydrogen bonding partners and an increase in hydrophobicity, due to replacing the charged guanidino nitrogen with a nonpolar amidino carbon, possibly makes water binding in this pocket less favorable.

1400W Complex. Inhibitor 1400W bears an amidine group that anchors the compound in the heme active site through hydrogen bonds with Glu 363 and the Trp 358 carbonyl oxygen (Figure 7). The benzyl ring is positioned just above the two heme propionate groups. There is no clearly defined electron density corresponding to the 3-aminomethyl group attached to the benzyl ring (Figure 5), although some residual electron density indicates that the amino nitrogen might interact with the propionate group from the pyrrole ring D. Because of the interaction with 1400W this propionate group is bent down from its normal position (Figure 7). It is puzzling (see Discussion) that the aminomethyl group of 1400W is disordered even though its potential hydrogen bonding partners, the heme propionate group(s), are within H-bonding distances.

DISCUSSION

Binding Mode of NO. One reason for determining the structure of the NO complex is that NO can serve as a mimic for the oxy complex. This is important in that, thus far, we have been unsuccessful in trapping the oxy complex in the crystalline state. In addition, the CO complex has presented some problems. Although the electron density maps for the CO complex reveal electron density occupying the distal coordination position, the lack of a clearly defined CO−iron bond and indications of disorder in the substrate precluded a detailed analysis of the CO complex. As a result, the NO complex is the only stable Fe^{2+}−diatomic ligand complex that we have been able to analyze crystallographically so far. Also, the NO complex is of interest since NO is a product NOS catalysis and an inhibitor of NOS under steady-state conditions. As such, the structure of the NO complex is of relevance to the catalytic mechanism. NO inhibits NOS activity since formation of the ferrous−NO adduct is faster than its decay resulting in 70−90% of nNOS accumulating as the inactive NO complex (*24*, *29*). NO thus operates as a competitive inhibitor and increases the apparent Km of O_2 to nNOS by a factor of 10 (*30*). In contrast to nNOS and iNOS, a recent study on eNOS (*31*) detected little buildup of heme−NO complex during NO synthesis from L-Arg as the heme reduction in eNOS is extremely slow owing to the slow electron-transfer rate from flavins to heme (*32*). The local concentration of NO is simply not high enough (>50 nM) to enable accumulation of the heme-NO complex. However, when NHA was directly used as the substrate, which produces a 3-fold faster rate of NO synthesis than does L-Arg, buildup of heme-NO complex did occur during steady-state catalysis.

Finally, it is important to assess the present crystal structure work in light of the wealth of spectroscopic data on NOS-ligand complexes. Both absorption and resonance Raman spectroscopic studies have been carried out on the NOS−NO adduct (*33*−*35*). Substrate binding to the nNOS−NO adduct causes an increase in the Fe−NO stretching frequency, indicating a direct hydrogen bonding interaction between substrate and iron-bound NO, which is consistent with the present crystal structure. In the absence of substrate, NO binding can sample multiple conformations, while the hydrogen bond between the guanidino nitrogen and NO oxygen stabilizes the bound NO in a unique orientation which was evidenced by sharpened hyperfine splitting of the NO complex EPR spectrum (*36*).

Expected O_2 Binding Mode. Although the extremely short lifetime of NOS−O_2 adduct (*37*) precluded us from solving

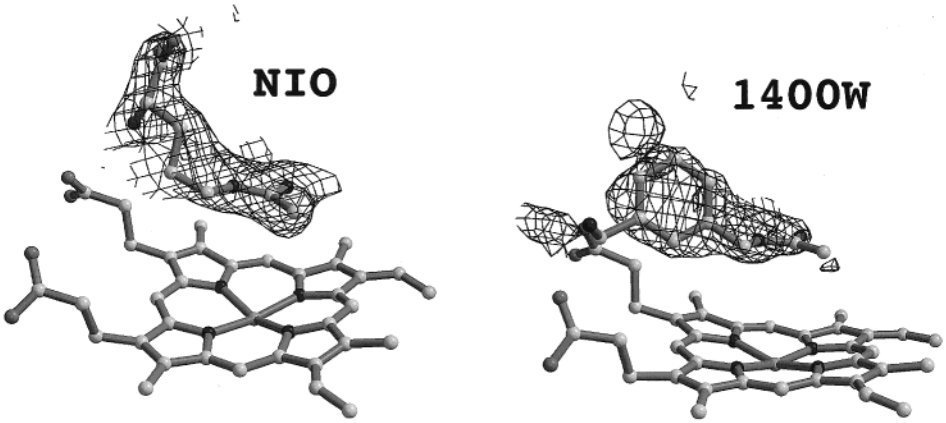

FIGURE 5: $2F_o - F_c$ omit maps of the NIO and 1400W complexes contoured at 1σ. These maps were generated by removing the inhibitor atoms followed by a round of simulated annealing refinement. Carbon atoms are light, nitrogen black, and oxygen dark gray. Note that the 3-aminomethyl group of 1400W has no well-defined electron density.

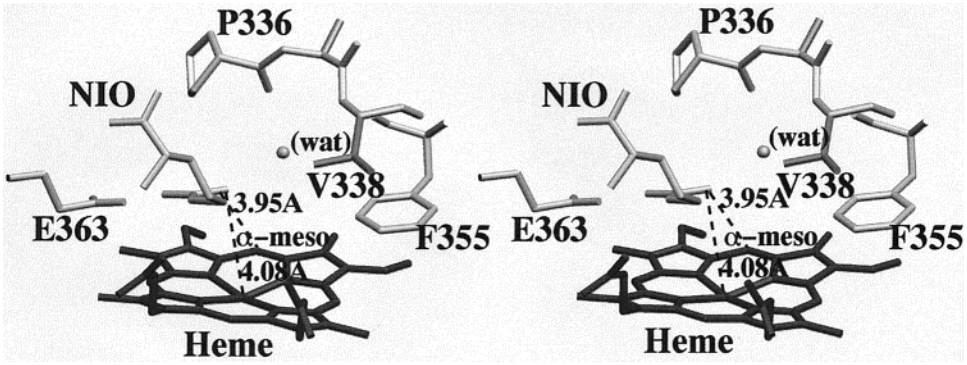

FIGURE 6: Stereo drawing of the heme active site of eNOS with NIO bound. Key contacts from the NIO amidino methyl carbon to the heme are labeled with corresponding distances. The water molecule displayed exists in the active site of the eNOS−Arg complex structure but is missing here, likely due to lack of hydrogen bonding partner from NIO.

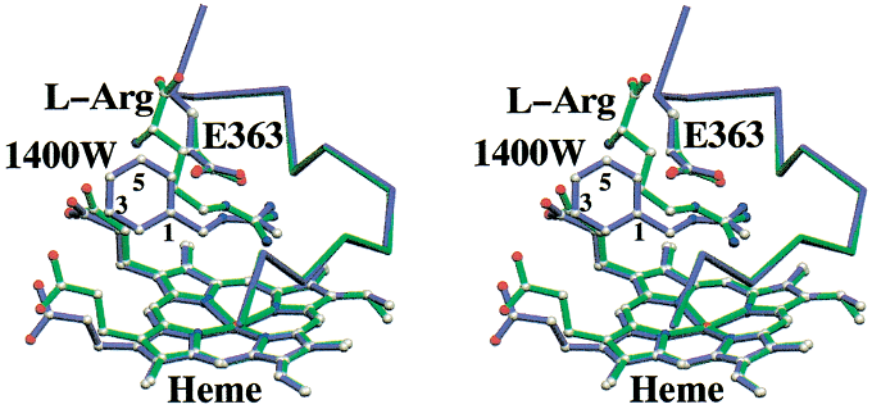

FIGURE 7: Stereo drawing of the eNOS−1400W complex (purple) superimposed on the eNOS-L-arg structure (green). The α-carbons of residues 353−364, along with the side chain of Glu363, are shown. The atom color schemes are the same as in Figure 2. The 3-position of the benzyl ring sits above and between two heme propionate groups, pushing the propionate of pyrrole ring D downward, although the 3-aminomethyl substituent is disordered in the structure and is not shown in the model.

the oxy complex structure, the recent structure of the ternary P450cam−substrate−O_2 structure (*38*), together with our present results, can provide insights on the most likely structure of the NOS oxy complex. In the P450-oxy complex, the dioxygen has a bend angle as large as 48°. If dioxygen adopts a similar bend angle in NOS then in the presence of substrate, dioxygen would bend over toward pyrrole ring C, similar to that observed for NO complex, and would contact the Phe 355 side chain. Crane et al. (*39*) noticed that the active site was crowded when they attempted to model a superoxide (O_2^-) in the NHA complex structure. Our present study shows that the substrate moves in order to accommodate the NO ligand and a similar motion is expected in the oxy complex. Despite the expected greater bend angle in the oxy complex compared to the NO complex, the guanidino nitrogen of L-Arg should still be in position to H-bond with dioxygen. That substrate binding slows the decay rate of O_2 (*37*) suggests a direct stabilization owing to substrate-oxygen interactions. The one problem with this argument is that unlike the NOS−NO adduct, the resonance Raman spectral features of the NOS−O_2 adduct are not influenced by the presence of substrate or pterin (*40*). The

Scheme 1

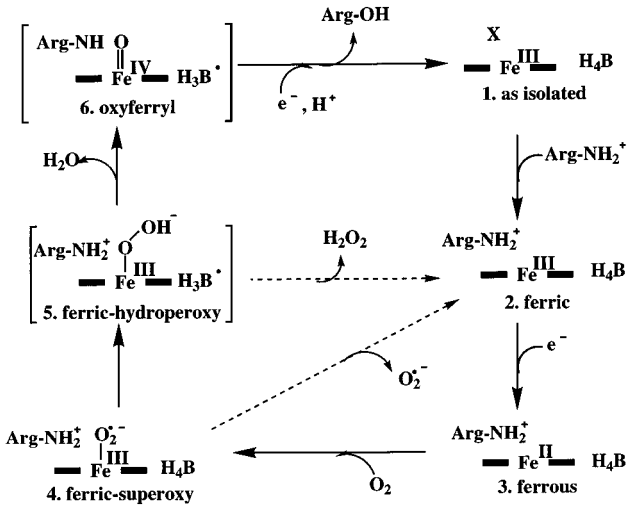

most probable explanation for the inability of substrate to alter the resonance Raman properties of the oxy complex is that O_2 is a polar molecule with one favored resonance structure that is unlikely to be altered by neighboring interactions (*40*).

Relevance to the Catalytic Mechanism. The most important insight of the present work on elucidating the mechanism of NOS catalysis is the expected H-bond formed between NO and the substrate. As proposed by Crane et al. (*10*), the substrate itself rather than some catalytic amino acid side chain or water provides the necessary proton required for cleavage of the O−O bond as illustrated in Scheme 1. In the absence of L-Arg and H_4B, the O−O bond cleavage will not proceed since the proton source, L-Arg, is absent and instead, the iron-bound O_2 is released as superoxide (*15*−*17*).

A plausible mechanism of H_4B/Arg-dependent inhibition of superoxide generation is illustrated in Scheme 1. In this mechanism dioxygen first binds to the ferrous iron to form [Fe^{II}-O_2], which is isoelectric to a ferric-superoxy species, [Fe^{III}-$O_2^{\bullet -}$] (4 in Scheme 1). The activation of dioxygen requires another electron which now is thought to derive from H_4B (*13*, *19*, *20*) resulting in ferric-hydroperoxy species, [Fe^{III}-OOH^-] (5 in Scheme 1). The ferric-hydroperoxy species further abstracts a proton from the guanidino nitrogen of L-Arg (*10*) to result in O−O bond cleavage, release of water, and formation of the high valency oxyferryl-like species, $[Fe{-}O]^{2+}$ (no. 6 in Scheme 1). Similar to cytochrome P450, this high valency intermediate is the species thought to be responsible for substrate hydroxylation. Without H_4B and L-Arg, the iron-bound O_2 will not have the electron and proton necessary for its activation and the superoxide radical is released. It should be cautioned, however, that in both P450 and NOS the oxyferryl species remains a hypothetical intermediate and has yet to be shown to be part of the productive catalytic cycle in either enzyme.

Mechanism-Based Amidine NOS Inhibitors. The one unexpected feature in the binding of 1400W was the lack of electron density corresponding to the aminomethyl group (Figure 5). One possible explanation is that the phenyl ring can adopt two conformations, resulting in the aminomethyl group pointing up or down (Figure 7). There also could be rotational disorder about the C−N bond. In addition, judging from these distances, the aminomethyl group should be capable of electrostatic interactions with either of the two propionate groups which could result in the aminomethyl group occupying multiple positions. We had anticipated that the 1400W amino group might mimic the α-amino group of L-Arg. However, it is clear from the observed phenyl group position, that the aminomethyl group cannot protrude into the pocket occupied by the α-amino group of L-Arg in the substrate complex, even when disorder is taken into account.

Both L-NIO and 1400W have the amidine functionality that mimics the guanidine of arginine in its H-bonding interactions with Glu 363. However, the replacement of a guanidino nitrogen with an amidino methyl carbon precludes these inhibitors from serving as substrates. Silverman and co-workers have systematically investigated the mechanism of inactivation of iNOS by L-NIO (*23*). These studies indicate that inactivation occurs after an oxidation step but prior to hydroxylation. The radiolabeled ligand binding experiments show that NIO inactivates iNOS by modifying the heme instead of the protein, leading to biliverdin IX as the major heme degradation product. These authors proposed two inactivation mechanisms (*23*). In the first mechanism, the inability of NIO to donate a proton to the ferric-hydroperoxy intermediate (nos. 5-to-6 in Scheme 1) leads to excess production of peroxide and heme destruction. In the second mechanism, the hydroperoxy-heme abstracts a hydrogen atom from the NIO terminal methyl carbon, thus forming a carbon radical which attacks the heme *meso*-carbon to give a heme-NIO adduct that initiates a series of reactions leading to the final product, biliverdin IX.

From the structural perspective, the first mechanism is more feasible than the second because the second mechanism requires a covalent bond between NIO and heme, which is not consistent with the stable binding mode observed in the crystal structure. Being almost identical to the mode of L-Arg binding, NIO binds in the heme distal pocket with its methyl group pointing toward the heme iron. Although some of the NIO could be bound with the terminal nitrogen close to the heme, explaining the small amount of N^{ω}-hydroxy-NIO observed (*23*), this binding mode must represent a very small population of bound NIO. In the binding mode we observe in the crystal structure, in both subunits the methyl carbon of NIO is closest to the heme pyrrole nitrogen of ring B (3.6−3.7 Å) and as far as ∼4.0 Å from the α-*meso*-carbon. Formation of a NIO-heme covalent bond would thus require disruption of hydrogen bonds between NIO and surrounding protein groups. This requires that the lifetime of the radical would be sufficient to allow disruption of these H-bonds and movement of NIO toward the *meso*-carbon for covalent bond formation.

The first mechanism, however, does not require movement of NIO. In the absence of the proper proton donor to the hydroperoxy intermediate, the mechanism of NOS switches to one similar to that proposed for human heme oxygenase (Scheme 2) which gives biliverdin IXα as the sole product (*41*). The mechanism proceeds via a hydroperoxy intermediate (*42*−*44*) that selectively hydroxylates the heme α-*meso*-carbon. Examination of the structural features of heme oxygenase (*45*) reveals a close packing of the distal helix against the heme plane, which leaves only the α-*meso* heme carbon available for hydroxylation. In addition, potential H-bonding interactions favor a bending of dioxygen toward

Scheme 2[a]

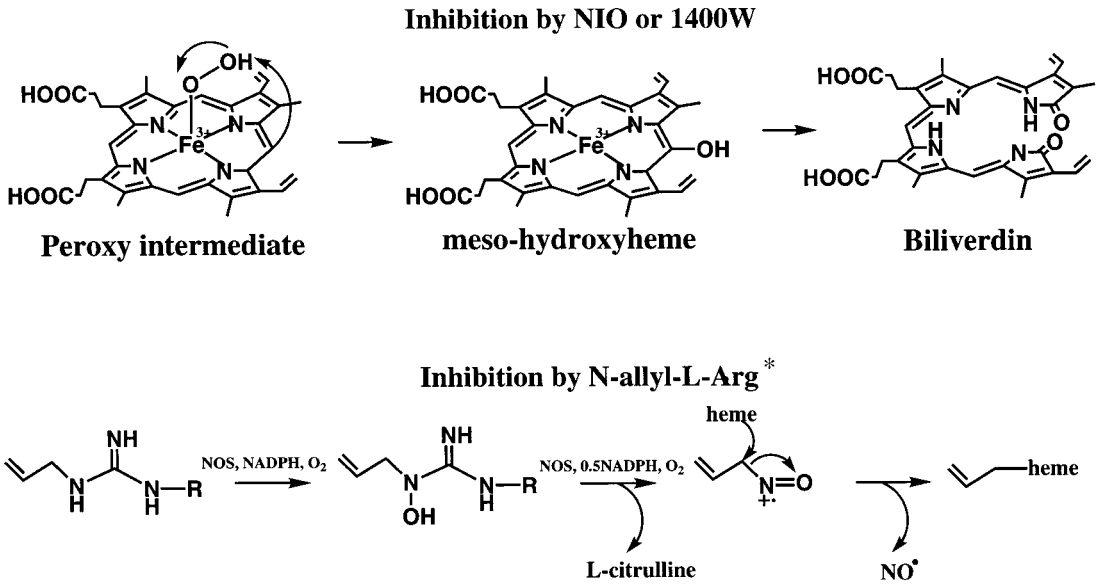

[a] (∗) The scheme is adopted from ref *22*.

the α-*meso*-heme carbon. The NIO bound to the NOS active site could fulfill these requirements for catalyzing heme oxygenase activity by slowing the rate of O−O bond cleavage relative to hydroxylation of a heme *meso*-carbon since there is no nearby proton source required for cleavage of the peroxide O−O bond. This provides sufficient time for the peroxy intermediate to hydroxylate a heme *meso*-carbon, ultimately leading to biliverdin IXα formation.

The same inactivation mechanism can also operate with 1400W for it shares the same amidine group as does NIO and the amidine groups in both NIO and 1400W structures are bound in a similar fashion to the heme distal pocket. The fact that the inactivation of iNOS by 1400W is H_4B-independent implies that it is highly likely to follow the same heme oxygenase-type mechanism in which O−O bond cleavage is not necessary. It may at first seem surprising that 1400W was found to be an irreversible inactivator only to iNOS (*46*), since the active site structures of all three isoforms are so similar (*10*, *11*, *13*) (nNOS, unpublished). However, the selectivity of 1400W toward iNOS can be partly attributed to the higher turnover of iNOS compared to eNOS and nNOS, which leads to overproduction of peroxide and irreversible heme damage.

Mechanism-Based Guanidine NOS Inhibitors. Another class of mechanism-based inhibitors are those N^G-substituted L-arginine analogues. The most thoroughly characterized are N^G-monomethyl-L-arginine (NMMA) (*21*, *47*) and N^G-allyl-L-arginine (*22*, *48*), which bear a substituent bound to a terminal guanidinium N atom. Although these inhibitors also cause heme loss, the mechanism appears to be different as the final products are alkylated heme at *meso*-carbon positions with reduced porphyrin aromaticity (*22*) but not biliverdin IX (Scheme 2). Because the secondary amine, i.e., the substituted terminal guanidino nitrogen, still bears one proton, hydroxylation of this nitrogen is an intermediate for inactivation (*22*). The key difference in this class of inactivators from the amidine-bearing inhibitors discussed above is that the inactivation occurs after hydroxylation and the enzyme can still produce some NO and citrulline. This is identical to the process that produces NHA from substrate, L-Arg, in normal NOS catalysis. The subsequent step of inactivation, again similar to the conversion of NHA to L-citrulline and NO, involves the attack on the guanidino carbon by the ferric-peroxy species, releasing L-citrulline and NO while the alkyl- (or alkenyl-) radical covalently attaches to heme (*22*).

Although structures of NOS complexed with N^G-substituted-L-arginine have yet to be published, the available structures of L-Arg and *S*-alkyl-isothiourea complexes do provide suggestions of modes of binding of these inactivators to the active site. As noted in S-alkyl-isothiourea structures (*49*), the small N^G-alkyl- (alkenyl-) substituted group of inactivators could be accommodated in a hydrophobic patch defined by Phe 355 and Val 338 in eNOS. These additional nonbonded contacts improve binding to the active site, but would not significantly shift the position of the substituted guanidino nitrogen away from the heme iron. This precise location of the proton donor is important for turnover. *N*-Propargyl-L-arginine is a competitive inhibitor but not an irreversible inactivator (*50*), possibly because the rigid and bulky propargyl group would have an unfavorable steric clashing within the aforementioned hydrophobic patch that forces the substituted guanidino nitrogen to shift further from the heme iron. The N^G atom in this type of inactivator, such as N^G-monomethyl-L-Arg, N^G-allyl-L-Arg, and N^G-propyl-L-Arg, must be located near to the heme iron similar to the situation in L-Arg and is the reason these inactivations proceed with a mechanism so similar to that of normal NO synthesis. Actually, the normal turnover products, L-citrulline and NO, are indeed observed in these cases, although the enzyme itself is gradually inactivated due to the alkylation of heme by the N^G-alkyl (or alkenyl) substituents of the inactivator.

REFERENCES

1. Dinerman, J. L., Lowenstein, C. J., and Snyder, S. H. (1993) *Circ. Res. 73*, 217−222.
2. Griffith, O. W., and Stuehr, D. J. (1995) *Annu. Rev. Physiol. 57*, 707−736.

3. Nathan, C. (1997) *J. Clin. Invest. 100*, 2417−2423.
4. Knowles, R. G., and Moncada, S. (1994) *Biochem. J. 298*, 249−258.
5. Masters, B. S., McMillan, K., Sheta, E. A., Nishimura, J. S., Roman, L. J., and Martásek, P. (1996) *FASEB J. 10*, 552−558.
6. Bredt, D. S., Hwang, P. M., Glatt, C. E., Lowenstein, C., Reed, R. R., and Snyder, S. H. (1991) *Nature 351*, 714−718.
7. Hillier, B. J., Christopherson, K. S., Prehoda, K. E., Bredt, D. S., and Lim, W. A. (1999) *Science 284*, 812−815.
8. Cho, H. J., Xie, Q. W., Calaycay, J., Mumford, R. A., Swiderek, K. M., Lee, T. D., and Nathan, C. (1992) *J. Exp. Med. 176*, 599−604.
9. Nishida, C. R., and Ortiz de Montellano, P. R. (1998) *J. Biol. Chem. 273*, 5566−5571.
10. Crane, B. R., Arvai, A. S., Ghosh, D. K., Wu, C., Getzoff, E. D., Stuehr, D. J., and Tainer, J. A. (1998) *Science 279*, 2121−2126.
11. Fischmann, T. O., Hruza, A., Niu, X. D., Fossetta, J. D., Lunn, C. A., Dolphin, E., Prongay, A. J., Reichert, P., Lundell, D. J., Narula, S. K., and Patricia, C. W. (1999) *Nature Struct. Biol. 6*, 233−242.
12. Li, H., Raman, C. S., Glaser, C. B., Blasko, E., Young, T. A., Parkinson, J. F., Whitlow, M., and Poulos, T. L. (1999) *J. Biol. Chem. 274*, 21276−21284.
13. Raman, C. S., Li, H., Martásek, P., Král, V., Masters, B. S., and Poulos, T. L. (1998) *Cell 95*, 939−950.
14. Tayeh, M. A., and Marletta, M. A. (1989) *J. Biol. Chem. 264*, 19654−19658.
15. Vásquez-Vivar, J., Kalyanaraman, B., Martásek, P., Hogg, N., Masters, B. S., Karoui, H., Tordo, P., and Pritchard, K. A. J. (1998) *Proc. Natl. Acad. Sci. U.S.A. 95*, 9220−9225.
16. Xia, Y., Tsai, A.-L., Berka, V., and Zweier, J. L. (1998) *J. Biol. Chem. 273*, 25804−25808.
17. Pou, S., Keaton, L., Surichamorn, W., and Rosen, G. M. (1999) *J. Biol. Chem. 274*, 9573−9580.
18. Rusche, K. M., Spiering, M. M., and Marletta, M. A. (1998) *Biochemistry 37*, 15503−15512.
19. Bec, N., Gorren, A. C., Voelker, C., Mayer, B., and Lange, R. (1998) *J. Biol. Chem. 273*, 13502−13508.
20. Hurshman, A. R., Krebs, C., Edmondson, D. E., Huynh, B. H., and Marletta, M. A. (1999) *Biochemistry 38*, 15689−15696.
21. Olken, N. M., and Marletta, M. A. (1993) *Biochemistry 32*, 9677−9685.
22. Zhang, H. Q., Dixon, R. P., Marletta, M. A., Nikolic, D., Van Breemen, R., and Silverman, R. B. (1997) *J. Am. Chem. Soc. 119*, 10888−10902.
23. Fast, W., Nikolic, D., Van Breemen, R. B., and Silverman, R. B. (1999) *J. Am. Chem. Soc. 121*, 903−916.
24. Abu-Soud, H. M., Wang, J., Rousseau, D. L., Fukuto, J. M., Ignarro, L. J., and Stuehr, D. J. (1995) *J. Biol. Chem. 270*, 22997−23006.
25. Martásek, P., Liu, Q., Liu, J., Roman, L. J., Gross, S. S., Sessa, W. C., and Masters, B. S. (1996) *Biochem. Biophys. Res. Commun. 219*, 359−365.
26. Otwinowski, Z., and Minor, W. (1997) *Methods Enzymol. 276*, 307−326.
27. Brünger, A. T., Adams, P. D., Clore, G. M., DeLano, W. L., Gros, P., Grosse-Kunstleve, R. W., Jiang, J.-S., Kuszewski, J., Nilges, M., Pannu, N. S., Read, R. J., Rice, L. M., Simonson, T., and Warren, G. L. (1998) *Acta Crystallogr., Sect. D 54*, 905−921.
28. Jones, T. A. (1985) *Methods Enzymol. 115*, 157−171.
29. Wang, J., Stuehr, D. J., and Rousseau, D. L. (1995) *Biochemistry 34*, 7080−7087.
30. Abu-Soud, H. M., Rousseau, D. L., and Stuehr, D. J. (1996) *J. Biol. Chem. 271*, 32515−32518.
31. Abu-Soud, H. M., Ichimori, K., Presta, A., and Stuehr, D. J. (2000) *J. Biol. Chem. 275*, 17349−17357.
32. Miller, R. T., Martásek, P., Omura, T., and Masters, B. S. S. (1999) *Biochem. Biophys. Res. Commun. 265*, 184−188.
33. Wang, J., Rousseau, D. L., Abu-Soud, H. M., and Stuehr, D. J. (1994) *Proc. Natl. Acad. Sci. U.S.A. 91*, 10512−10516.
34. Hurshman, A. R., and Marletta, M. A. (1995) *Biochemistry 34*, 5627−5634.
35. Abu-Soud, H. M., Wu, C., Ghosh, D. K., and Stuehr, D. J. (1998) *Biochemistry 37*, 3777−3786.
36. Migita, C. T., Salerno, J. C., Masters, B. S., Martásek, P., McMillan, K., and Ikeda-Saito, M. (1997) *Biochemistry 36*, 10987−10992.
37. Abu-Soud, H. M., Gachhui, R., Raushel, F. M., and Stuehr, D. J. (1997) *J. Biol. Chem. 272*, 17349−17353.
38. Schlichting, I., Berendzen, J., Chu, K., Stock, A. M., Maves, S. A., Benson, D. E., Sweet, R. M., Ringe, D., Petsko, G. A., and Sligar, S. G. (2000) *Science 287*, 1615−1622.
39. Crane, B. R., Arvai, A. S., Ghosh, S., Getzoff, E. D., Stuehr, D. J., and Tainer, J. A. (2000) *Biochemistry 39*, 4608−4621.
40. Couture, M., Stuehr, D. J., and Rousseau, D. L. (2000) *J. Biol. Chem. 275*, 3201−3205.
41. Maines, M. D. (1988) *FASEB J. 2*, 2557−2568.
42. Wilks, A., Torpey, J., and Ortiz de Montellano, P. R. (1994) *J. Biol. Chem. 269*, 29553−29556.
43. Wilks, A., and Ortiz de Montellano, P. R. (1993) *J. Biol. Chem. 268*, 22357−22362.
44. Davydov, R. M., Yoshida, T., Ikeda-Saito, M., and Hoffman, B. M. (1999) *J. Am. Chem. Soc. 121*, 10656−10657.
45. Schuller, D. J., Wilks, A., Ortiz de Montellano, P. R., and Poulos, T. L. (1999) *Nat. Struct. Biol. 6*, 860−867.
46. Garvey, E. P., Oplinger, J. A., Furfine, E. S., Kiff, R. J., Laszlo, F., Whittle, B. J., and Knowles, R. G. (1997) *J. Biol. Chem. 272*, 4959−4963.
47. Olken, N. M., Osawa, Y., and Marletta, M. A. (1994) *Biochemistry 33*, 14784−14791.
48. Olken, N. M., and Marletta, M. A. (1992) *J. Med. Chem. 35*, 1137−1144.
49. Li, H., Raman, C. S., Martásek, P., Kral, V., Masters, B. S. S., and Poulos, T. L. (2000) *J. Inor. Biochem. 81*, 133−139.
50. Fast, W., Levsky, M. E., Marletta, M. A., and Silverman, R. B. (1997) *Bioorg. Med. Chem. 5*, 1601−1608.

BI002658V